Astron. Astrophys. 340, 265–276 (1998)

ASTRONOMY AND ASTROPHYSICS

Temperature and density diagnostics of quiet Sun and active regions observed with CDS NIS

E. Landi[1] **and M. Landini**[1]

Department of Astronomy and Space Science, University of Florence, Italy

Received 19 February 1998 / Accepted 15 September 1998

Abstract. We study the Differential Emission Measure distribution of two pairs of active and quiet regions of the solar atmosphere, observed by CDS Normal Incidence Spectrometer (NIS) on SOHO, and investigate their temperature and density structure . Use is made of the Arcetri Method (Landi & Landini 1997) for DEM and density diagnostics. An iterative method for determining the DEM is presented; it allows to select physically meaningful DEM distributions having a definite top temperature along the line of sight. Density sensitive lines are identified and density diagnostics is performed for all the four different spectra. Comments are made on the density versus temperature curves obtained for each region. Simple constant pressure models are not satisfactory and constraints on temperature and density distributions are discussed.

Key words: Sun: activity – Sun: atmosphere – Sun: corona – Sun: UV radiation

1. Introduction

The Coronal Diagnostic Spectrometer (CDS) on Soho is a grazing/normal incidence spectrograph, aimed to produce stigmatic spectra of selected regions of the solar surface in six spectral windows of the extreme ultraviolet from 150 Å to 785 Å (Harrison et al. 1995).

This spectral band is extremely rich in emission lines of a large number of highly ionized ions of the most abundant elements and its study represents a precious tool for a detailed diagnostic of temperature, density and chemical composition of the solar transition region and corona. Moreover it is a unique laboratory for testing atomic physics models and theoretical calculations of collision rates and transition probabilities.

The large number of emission lines that are observed in the solar spectrum, coupled to the large amount of atomic data now available (ADAS - Summers et al. 1996, CHIANTI - Dere et al. 1997, The Arcetri Spectral Code - Landi & Landini 1998) and a new temperature and density diagnostic technique (Landi & Landini 1997, hereafter Paper I), permit to do a detailed temperature and density diagnostics of the solar transition region and corona.

Send offprint requests to: E. Landi

In the present paper we have applied this technique to the intensities of lines emitted by Active and Quiet Regions of the solar atmosphere observed with the CDS Normal Incidence spectrograph, and comparison are performed among temperature and density models of the different sources.

2. The theoretical method

2.1. Differential emission measure determination

Several methods for calculating the *Differential Emission Measure* have been developed, using different algorithms and approximations; a comprehensive description of the most important ones and a critical assessment and comparison of their reliability in connection with the Coronal Diagnostic Spectrometer on SOHO can be found in Harrison & Thompson (1992).

We used a new method to evaluate the *Differential Emission Measure* which adopts an iterative procedure described in paper I and uses density independent lines.

Here we present a very brief summary of the theoretical method. For further details we refer the reader to paper I.

The flux emitted by a thin plasma in a line is given by

$$F_{ij} = \frac{1}{4\pi d^2} \int_h N_j\left(X^{+m}\right) A_{ij} dV \qquad ph\ cm^{-2}\ s^{-1} \tag{1}$$

where $N_j(X^{+m})$ is the number density population of level *j* of ion X^+, A_{ij} is the radiative probability to decay to level *i* and d is the distance of the source.

We can define the *Contribution Function* as follows:

$$G_{ij}(T, N_e) = \frac{N_j(X^{+m})}{N(X^{+m})} \frac{N(X^{+m})}{N(X)} \frac{N(X)}{N(H)} \frac{N(H)}{N_e} \frac{A_{ij}}{N_e} \tag{2}$$

The following definition of the *Volume Differential Emission Measure* $\varphi(T)$ is assumed

$$\varphi(T) = N_e^2 \frac{dV}{d\,T} \tag{3}$$

A trial *Differential Emission Measure* $\varphi_o(T)$ is adopted; using a *Correction Function* $\omega(T)$, the true *Differential Emission Measure* is

$$\varphi(T) = \omega(T)\ \varphi_o(T) \tag{4}$$

The effective temperature T_{eff} can be defined as

$$LogT_{eff} = \frac{\int G_{ij}(T)\ \varphi_o(T)\ logT\ dT}{\int G_{ij}(T)\ \varphi_o(T)\ dT} \quad (5)$$

It may be easily shown that, as long as the correction function is slowly varying,

$$I_{ij} = \frac{1}{4\pi}\ \omega(T_{eff})\ \int\ G_{ij}(T)\ \varphi_o(T)\ dT \quad (6)$$

Using Eq. 6 for several lines with different T_{eff} the correction $\omega(T_{eff})$ for each line may be computed and a new approximated *Differential Emission Measure* $\varphi(T_{eff})$ evaluated.

A spline function is drawn through the $\varphi(T_{eff})$ and this function is taken as the new trial *Differential Emission Measure* . Then the procedure is repeated until either the $\omega(T_{eff})$ are all equal to 1 within the errors, or the best χ^2 is reached.

The program is also allowed to constrain *Differential Emission Measure* distribution having a top temperature T_{max}.

The high temperature behaviour of the *Differential Emission Measure* distribution deserves some comment; it is usually accepted that the *Differential Emission Measure* tends to very low values for high temperature, but this is in clear disagreement with the natural observation that the temperature along the line of sight should have a maximum value; this means that the range of temperature values is limited to a top value T_o where the $\varphi(T_o)$ is infinite. As long as no physical constraint is posed on the *Differential Emission Measure* solutions, the way followed by the *Differential Emission Measure* divergence is completely arbitrary.

We have selected an asyntothic function $\frac{1}{\sqrt{(T_o^p - T^p)}}$ to simulate solutions of very crude loops models obtained solving the energy equation. (Landini & Monsignori Fossi 1975)

The transformation of variables

$$\left(\frac{T}{T_o}\right)^p = sin^2\theta \quad (7)$$

easily allows to take correctly into account the divergence when doing the integration of the *Contribution Functions* over the *Differential Emission Measure* .

The analytical shape is assumed to hold for the last dex of log T and both T_o and *p* are allowed to change to select the best fit to the observations.

Fig. 5 shows examples of such a type of solution, which are discussed in Sect. 4.3.

2.2. The density evaluation

We used the temperature and density diagnostic procedure shown in Paper I, that is briefly summarised in this section.

With a good approximation it is usually possible to put $G_{ij}(T, N_e)$ as

$$G_{ij}(T, N_e) = f_{ij}(N_e, T)\ g(T) \quad (8)$$

where $g(T)$ is function of temperature alone, identical for all the lines of the same ion and mainly due to the ionization equilibrium; $f_{ij}(N_e, T)$ is mainly determined by the population of the upper level and differs very little from a linear function of log T in the range of temperature values where the line is formed.

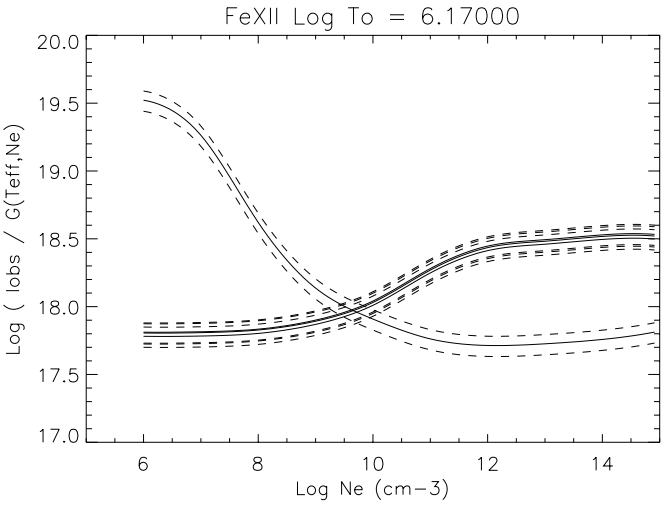

Fig. 1. Fe XII lines observed in CDS NIS 1 spectral range. The overlapping lines are the 346.8 Å, 352.1 Å and 364.4 Å transitions while the crossing one is the 338.2 Å transition. The Log T_{eff} is also shown at the top.

A new effective temperature T_{eff} may be evaluated

$$LogT_{eff} = \frac{\int g(T)\ \varphi(T)\ logT\ dT}{\int g(T)\ \varphi(T)\ dT} \quad (9)$$

and an *effective emission measure* $L_{ij}(N_e)$ may be computed as

$$L_{ij}(N_e) = \frac{I_{obs}}{G_{ij}(T_{eff}, N_e)} \quad (10)$$

The diagnostic method relies on the observation that if we plot all the L-functions measured for the same ion versus the electron density all the curves should meet in a common point $(N_e^\star, L(N_e^\star))$ provided that all the lines are formed at the same density. Moreover the L-functions of density independent lines must overlap and cross the same point as the others.

An example is given in Fig. 1.

For each ion, the effective temperature T_{eff} for each line is evaluated and the L-functions are displayed at that effective temperature versus electron density in order to verify line overlapping (for density independent lines) or proper crossing (for density dependent ones).

This method of analysis is effective when a large amount of theoretical data is available. In the present work we adopt the theoretical data of the new version of the Arcetri Spectral Code (Landi & Landini 1998). The element abundances reported in Feldman et al. 1992 have been used. The adopted relative ion population comes from Arnaud & Rothenflug 1985 for all the most abundant elements, and from Arnaud & Raymond 1992 for iron while the ion population of the less abundant elements has been taken from Landini & Monsignori Fossi 1991.

3. The observation

The Coronal Diagnostic Spectrometer on SOHO is composed of two different instruments, namely the Grazing Incidence Spectrometer (GIS) and the Normal Incidence Spectrometer (NIS). The GIS is equipped with a concave reflection grating and the spectrum is dispersed on four microchannel plates and spiral anode detectors covering four spectral ranges: 151-221, 256-341, 393-492 and 659-785 Å. In this study we have limited our attention only to the NIS wavelength bands, covering the ranges 307-379 and 513-633 Å. Full details of the CDS spectrometer can be found in Harrison et al. 1995.

Both the CDS spectrometers were calibrated before launch; details on the pre-flight calibration are reported in Bromage et al. 1996. Landi et al. 1997 have shown that NIS intensity calibration requires some corrections and propose that the relative calibration of NIS 1 and NIS 2 should be revised, NIS 1 intensities relative to NIS 2 being higher by a factor approximately three than expected, and that both NIS 1 and NIS 2 intensities require a slight wavelength dependent correction. In the present work, we adopt the standard intensity calibration included in the CDS software, but apply the corrections suggested by Landi et al. 1997. Line emission data are in erg cm^{-2} s^{-1} arcsec^{-2} and have been converted into flux for the *Differential Emission Measure* analysis. It is important to note that we are analysing the same dataset used by Landi et al. 1997; the difference between this work and the former one is that Landi et al. 1997 concerned instrumental calibration and used the spectrum of the whole observation, while in the present work we will consider the analysis of selected portions of the observed region to distinguish between active and quiet conditions. The present study therefore provides also a detailed check of the proposed corrections to the NIS intensity calibration.

The observation we have analysed is part of the NIS atlas observing program (NISAT_S) and was taken on 9 April 1996 (datafile s524r00). The slit used has dimension of $2^{"} \times 240^{"}$. The observation is composed by ten subsequent exposures obtained shifting the image on the slit of $2^{"}$ along the equator. The total area covered by the spectrometer is therefore $20^{"} \times 240^{"}$. The exposure time for each position was 50s. This exposure time is suitable both to achieve a satisfactory number of counts for all the lines necessary for this study and to avoid saturation for the brightest lines of the spectrum.

The observed emitting region is displayed in Fig. 2, where six monochromatic images are shown, each centred on top of a strong emission line. The lines have been chosen from several ions whose maximum abundance temperature is 10^5 K (O III), $10^{5.4}$ (O V), $10^{5.6}$ K (Ne VI and Ne VII), $10^{5.9}$ K (Mg VIII), $10^{6.0}$ K (Mg IX) and $10^{6.4}$ K (Fe XVI). The observed region shows the presence of a hot central structure surrounded by cooler plasma at both edges. The two cooler regions (one northward and the other southward of the central structure) show spectral features typical of quiet Sun, with a lower overall intensity and the weakness or absence of the hot Fe XVI 335.4 Å and 360 Å lines.

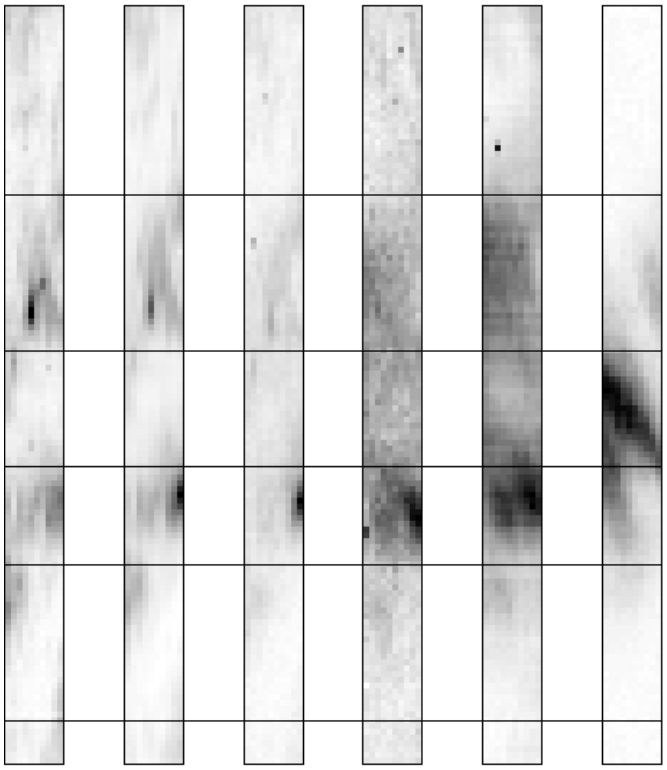

Fig. 2. Images of the emitting region (from left to right): O III (599.59 Å), O V (629.73 Å), Ne VI-VII (562.80 Å), Mg VIII (315.02 Å), Mg IX (368.06 Å) and Fe XVI (360.76 Å).

The hot region shows quite a complex structure, which changes as the ion's peak temperature rises. The emission of the transition region ions (up to He II, O V, Ne VII and Mg VI) is peaked in restricted areas a few arcseconds wide, one of which, around (-4$^{"}$,250$^{"}$), is relatively very strong. Hot coronal ions like Fe XV, Fe XVI, Mg IX, Mg X, Si XI and Si XII generate strong lines only in the central area, broadly overlapping the region showing Fe XVI line emission. Fe XVI lines (the hottest of this spectrum) are confined in an elongated region, which ends right over the strong transition region ions spot at (-4$^{"}$,250$^{"}$). The other ions show a more confused pattern. Further work is in progress in order to understand whether this Fe XVI structure can be identified as single coronal loop.

In the present work we have selected four portions from the total observed region, in order to obtain four different spectra, two of which centered on the active area and the other two in quiet Sun. We separated the Fe XVI elongated structure and averaged the observed emission in order to study its temperature, density and *Differential Emission Measure* . This selected portion of the image corresponds to the central segment in Fig. 2. We have also averaged the emission coming from the remaining of the area in which Fe XVI is still visible (segment below the elongated structure), and we have separated the two cooler regions at the top and at the bottom of the active area averaging their emission in order to obtain two different quiet Sun spectra. The uppermost section in Fig. 2 has not been considered.

For most of the lines observed both in the active and in the quiet sections of the observation the number of observed counts is high enough to give errors of a few percent. The experimental uncertainties on the measured fluxes are therefore much lower than the accuracy of the theoretical data. Several sources of uncertainty occurs in the calculation of the theoretical Contribution Functions. These include the element abundances, the ions abundances and the radiative and collisional transition probabilities for the level population calculations. We believe that all these factors contribute to limiting the accuracy of any diagnostic studies, and that it is important to take them into account when the experimental errors fall to very low values such as those provided by the present observation. For this reason we have associated a standard error to all the observed fluxes, and used these values in all the subsequent analysis. We estimate that a reasonable uncertainty for the theoretical data is 20%. For cases where the observed uncertainty of some very weak lines is greater than this value, the original error has been maintained.

4. Results

4.1. The differential emission measure

The plasma *Differential Emission Measure* was evaluated using either the maximum temperature option and the usual *Differential Emission Measure* definition over the temperature interval 10^4 to 10^8 K.

The lines used for the *Differential Emission Measure* study are reported in Table 1.

Fig. 3 shows an example of the *Differential Emission Measure* obtained for one active and one quiet Sun spectrum without the maximum temperature option. Both the quiet Sun regions show very similar temperature distribution, with a rather sharp peak around 1.25×10^6 K. The hotter lines (Fe XVI 335.4 Å and 360.7 Å) help to determine the shape of the curve for the higher temperatures, revealing that a very small amount of gas hotter than 1.6×10^6 K is required. Also the two active region spectra show a very similar *Differential Emission Measure* , and their peak temperature (around 1.6×10^6 K) is greater than the quiet Sun value, though the difference is not great. The curve shows a much broader maximum than the quiet Sun regions, and requires greater amounts of hot material. Each observed line is plotted in Fig. 3 at its effective temperature T_{eff} and its $\omega(T_{eff})\varphi(T_{eff})$.

It is important to note that in quiet Sun the high temperature behaviour of the *Differential Emission Measure* is mainly determined by the Fe XVI 360.76 Å since there are no other lines with similar effective temperature; moreover the other Fe XVI line at 335.41 Å receives significant contributions from the blending Fe XII and Mg VIII lines which lower its effective temperature T_{eff}. The problem is that the Fe XVI 360.76 Å line is probably blended with the strong Fe XI second order lines 180.41 Å and 180.60 Å. In active Sun conditions the contributions of these two lines are negligible, but in quiet regions they could provide some significant contribution to the total intensity of the Fe XVI line. This means that the high temperature tail of the quiet Sun *Differential Emission Measure* curves (such as the one reported in Fig. 3 left) could be overestimated. Unfortunately it is possible to determine only a very rough estimate of the Fe XI contribution to the 360.76 Å line comparing it with the 335.41 Å line because of the lack of the second order calibration for the NIS 1 spectrometer and because the Fe XVI 335.41 Å line is blended. Fe XI contribution seems to be smaller than 15 % of the total intensity in both the quiet Sun spectra.

4.2. The chemical composition

In the present study it is possible to check the relative abundances of nearly all the observed elements. If a systematic effect is present for ions of the same element, the points dispersion in Fig. 3 and their disagreement from the *Differential Emission Measure* may be reduced correcting the chemical composition of the emitting plasma.

The NIS spectral range includes several oxygen and neon lines which allow to check the relative Ne-O abundance using O IV, O V, Ne IV and Ne V lines; this is made possible by the fact that their effective temperatures T_{eff} are very close. These elements do not show great problems, nevertheless there is some difference between the adopted relative abundances and those observed in the present work. The adopted neon value seems to be slightly higher than observed relatively to oxygen. The difference is $\approx$ 20 %, and does not show significant variations in the four studied regions.

In all the four spectra problems arise with all the Mg V, VII and VIII lines, which usually do not agree with lines from other element's ions with similar temperature. The theoretical intensity of these magnesium lines is too strong if compared with the observed one. On the contrary Mg IX and Mg X show a more regular behaviour, with a better agreement with the iron and aluminum ions. This has some consequences also on the shape of the *Differential Emission Measure* itself since these magnesium lines help in determining the minimum of the *Differential Emission Measure* at around $10^{5.7}$ K in Figs. 3. There is also some evidence that the magnesium discrepancies are different in the four spectra, suggesting that the chemical composition of the emitting plasma is not homogeneous.

It is interesting to notice that Mg IX and X effective temperature T_{eff} is very close to the Fe X-XI and Al X-XI values. On the contrary ions from Mg V to Mg VIII fall in the effective temperature range covered by the neon ions Ne V to Ne VII. This means that Mg IX and Mg X are compared with Fe and Al and therefore the agreement found between these ions in the *Differential Emission Measure* study reflects the fact that the Mg/Fe and Mg/Al abundance ratios are in reasonable agreement with the Feldman 1992 values we have adopted. On the contrary the disagreement between Mg V to VIII and the neon ions is most probably due to some difference between the adopted Mg/Ne abundance ratio and the real one. The variations of these ratios with solar position is a signature of variations of the chemical composition of the emitting plasma, as already noted by Young & Mason 1997 analysing quiet and active region spectra observed by CDS-NIS.

Table 1. Lines used for the *Differential Emission Measure* study. Intensities are in 10^{-12} erg cm^{-2} s^{-1} arcsec^{-2}.

Ion	Wvl (Å)	Intensity			
		Quiet Sun 1	Quiet Sun 2	Active Sun 1	Active Sun 2
Fe XV	312.526	–	–	212±42.4	112±30.3
Mg VIII	313.824	295±59	396±79.2	1137±227	1261±252
Mg VIII	315.035	679±136	850±170	3161±632	2835±567
Mg VIII	317.042	149±29.8	294±58.8	781±156	690±138
Fe XV	327.062	–	–	446±89.2	201±40.2
Al X	332.835	597±119	910±182	1906±381	1886±377
Fe XVI	335.407	619±124	516±103	18679±3754	8713±1743
Mg VIII	339.090	151±30.2	227±45.4	652±130	718±144
Fe XI	341.217	301±60.2	474±94.8	997±199	1043±209
Fe X	345.779	581±116	771±154	1528±306	1757±351
Mg V	351.115	–	48.6±9.7	99.1±19.8	104±38.0
Mg V	353.235	–	–	246±49.2	165±33
Mg V	354.268	–	–	98.7±19.7	79.1±38.8
Mg V	355.603	–	79.5±15.9	–	–
Ne V	359.396	93.8±18.8	138±27.6	486±97.2	485±97.0
Fe XVI	360.749	181±36.2	125±25	8751±1750	3865±773
Mg VII	363.806	49.9±12.3	143±28.6	297±59.4	284±56.8
Mg VII	365.205	113±22.6	165±33	738±148	644±129
Mg VII	367.665	273±54.6	431±86.2	1489±298	1414±283
Mg IX	368.029	4867±973	6514±1302	16494±3299	16794±3359
O III	373.693	16.3±8.4	22.6±20.2	92.3±18.5	92.6±18.5
O III	374.030	70.7±14.1	126±25.2	277±55.4	229±45.8
O III	374.306	38.7±7.7	59.0±11.8	115±23	105±21
He I	515.373	130±26.0	226±45.2	586±117	509±102
Si XII	520.492	264±52.8	463±92.6	4599±920	3392±678
He I	522.018	268±53.6	450±90	1195±239	1030±206
O III	525.636	216±43.2	316±63.2	578±116	563±113
Ne IV	541.033	43.6±8.7	58.2±11.6	–	–
Ne IV	542.027	84.0±16.8	105±21	185±37	198±39.6
Ne IV	543.847	134±26.8	200±40	334±66.8	326±65.2
Al XI	550.015	239±47.8	406±81.2	1533±307	1360±272
O IV	553.293	379±75.8	556±111	950±190	959±192
O IV	554.032	620±124	876±175	1681±336	1524±305
O IV	554.487	1909±382	2845±569	4872±974	4921±984
O IV	555.247	426±85.3	605±121	1045±209	1019±204
Ca X	557.733	391±78.2	553±110	1514±303	1495±299
Ne VI	558.587	162±32.4	257±51	552±110	506±101
Ne VII	560.072	–	–	59.8±13.5	55.5±14.9
Ne VII	561.680	49.7±9.9	104±20.8	237±47.4	204±40.8
Ne VI	562.791	234±46.8	413±82.6	881±176	832±166
Si III	566.458	32.7±6.5	43.2±8.6	112±22.4	76.5±15.3
Ne V	569.790	82.1±16.4	136±27.2	264±52.8	252±50.4
Ne V	572.331	122±24.4	232±46.4	380±76	399±79.8
He I	584.334	10080±2016	17924±3585	46123±9225	40474±8095
O III	597.773	28.3±5.7	34.1±6.8	76.4±15.3	71.1±14.2
O III	599.565	511±102	696±139	1174±235	1198±240
O IV	608.354	282±56.4	408±81.6	746±149	720±144
Mg X	609.747	3610±722	4946±989	13321±2664	12517±2503
Mg X	624.897	1864±373	2359±472	6906±1381	6299±1260
O V	629.698	5975±1195	8258±1652	17052±3410	15319±3064

In order to evaluate the best chemical composition, neon and oxygen abundances have been changed, new *Differential Emission Measure* distributions evaluated and the mean χ^2 monitored to select the best solution.

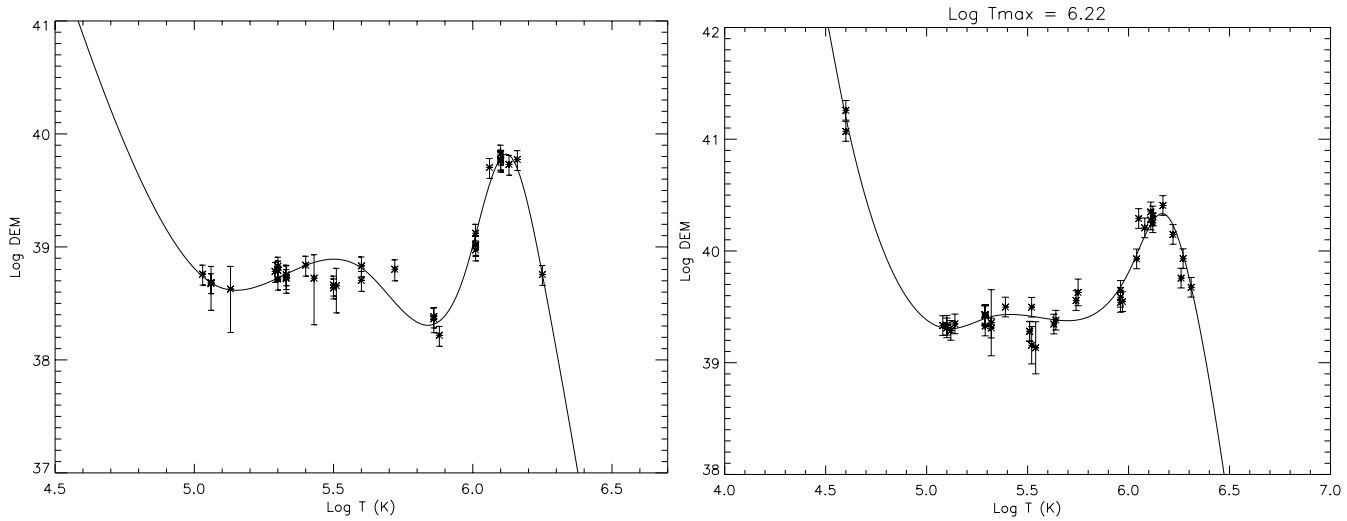

Fig. 3. Left: *Differential Emission Measure* of one of the two quiet Sun spectra in the s524 image. The mean χ^2 is 4.8. Right: *Differential Emission Measure* of one of the two active Sun spectra in the s524 image. The mean χ^2 is 2.5.

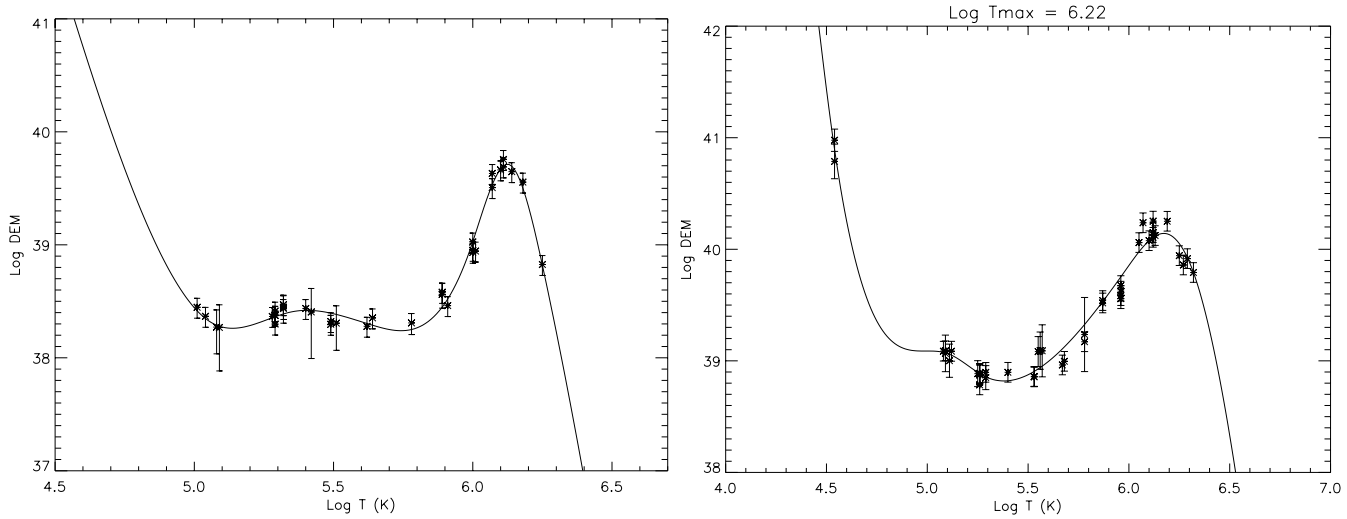

Fig. 4. Left: *Differential Emission Measure* obtained for one of the two quiet regions. The mean χ^2 is 0.61. Right: *Differential Emission Measure* obtained for one of the two active regions. The mean χ^2 is 1.0. In both spectra the neon and oxygen abundances have been changed.

The correction factor for neon is suggested by the Mg V - Ne V lines since their T_{eff} values are nearly identical, while the values of Ne VI, Ne VII, Mg VII and Mg VIII are slightly different and this may reflect in inaccuracies in the choice of the abundance correction factor. Anyway this choice was not easy because Ne V lines are observed both in NIS 1 and NIS 2, and these two groups agree only marginally with each other even after having allowed for the NIS 1 - NIS 2 intercalibration correction adopted in the present study. For this reason the abundance variation to be applied to neon and oxygen depends on which group of lines we used for evaluating the Mg V/Ne V differences. We chose to use the NIS 1 359.38 Å since its closeness in wavelength with the Mg V lines prevents any uncertainty in the NIS 1 - NIS 2 relative intensity calibration. Moreover, as pointed out by Young et al. 1998 studying the SERTS 89 active region spectrum (Thomas & Neupert 1994), no atomic physics problems seem to affect this line.

At the end of the procedure for the active region spectrum the neon abundance was increased by a factor 2.4, and the oxygen abundance was increased of a factor 3.0; in quiet Sun the neon abundance has been raised by a factor 2.0 and the oxygen value by a factor 2.5. Fig. 4 shows the resulting *Differential Emission Measure* ; these pictures should be directly compared with Fig. 3 since the two emitting regions analysed are the same. The χ^2 are given in the figure captions and clearly show the better agreement obtained with the new chemical composition. In Fig. 4 also lines from Mg VII have been used, despite their relatively weak density dependence. The agreement between neon and oxygen lines is now excellent, especially between Ne IV and O IV lines. The shape of the *Differential Emission Measure* is slightly different; this is due to the fact that the differences in

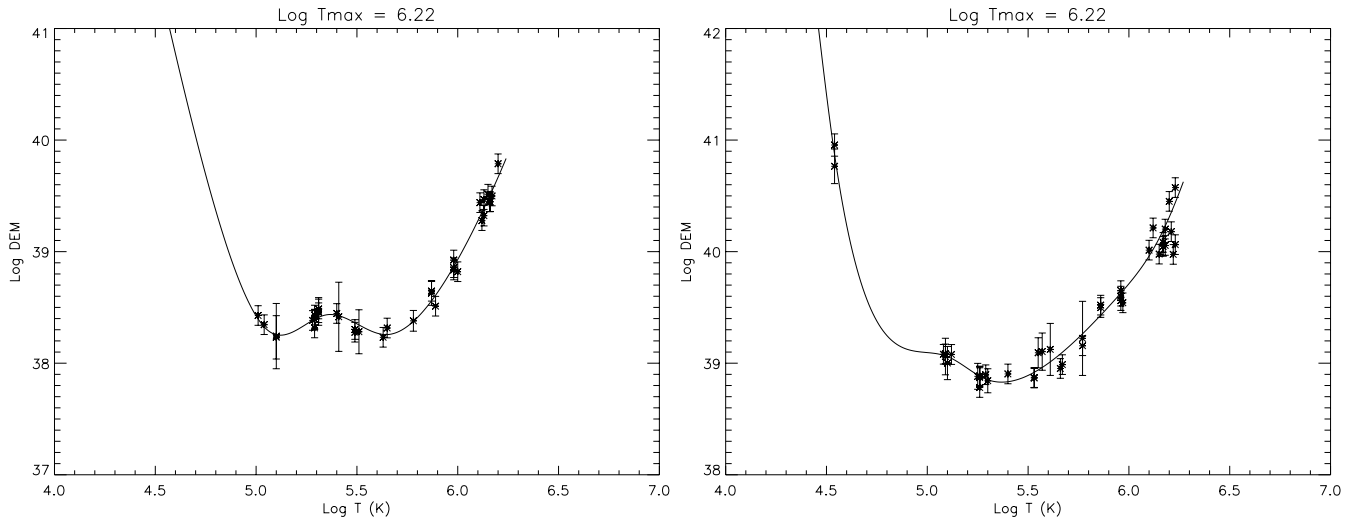

Fig. 5. Left: *Differential Emission Measure* of one of the two quiet Sun spectra in the s524 image, determined using the maximum temperature option. Right: *Differential Emission Measure* of one of the two active Sun spectra in the s524 image, determined using the maximum temperature option.

the oxygen and neon abundances used for determining the Fig. 3 solution forced the *Differential Emission Measure* to show a relatively small minimum around Log T $\simeq$ 5.7 K and to present a second maximum at Log T $\simeq$ 5.4 K, necessary to reproduce the O IV, O V, Ne IV and Ne V lines. This maximum has now disappeared. The agreement between magnesium and neon is now much better than in Fig. 3, and Ne VI, Ne VII, Mg VII and Mg VIII all lie on the same smooth curve.

Fig. 6 shows the comparison between the observed intensities used for the *Differential Emission Measure* studies and their theoretical values obtained using the *Differential Emission Measure* determined with the modified Feldman 1992 abundances. A very good agreement is found and it is possible to see that all the theoretical intensities reproduce the corresponding experimental values within the uncertainties.

4.3. The maximum temperature option

The maximum temperature option described in Sect. 2.1 has been applied to the same set of data. Fig. 5 reports examples of its effect on the determination of the *Differential Emission Measure* in quiet and active Sun.

The high temperature quiet Sun emission lines are well reproduced by the calculated *Differential Emission Measure* also in the temperature region of analytical approximation, revealing a maximum temperature around 1.6×10^6 K. The highest temperature line is Si XII 520.66 Å while Fe XVI 360.76 Å has been omitted because of the blending Fe XI second order line. This has been made necessary since the choice of the maximum temperature is very sensitive to small changes in the observed intensity of a line and the absence of information concerning the second order contribution does not allow to properly include the Fe XI line in the total theoretical Contribution Function.

A similar study has been performed also on the two active region spectra, this time including also the Fe XVI 360.76 Å line and the Fe XV 327.01 Å line, which was not available in quiet Sun. In the adopted maximum temperature range (1.7×10^6 to 2.2×10^6) these two lines are never able to agree for any value of the effective temperature, the Fe XV line being too weak relatively to the Fe XVI ones. This discrepancy was absent in the *Differential Emission Measure* curves determined without the maximum temperature option because in that case the effective temperatures T_{eff} of these two ions were quite different so they influenced the *Differential Emission Measure* curve in different points; the maximum temperature option instead forces both ions to be close to the maximum temperature of the curve and so they can be compared together. The simplest way to avoid this problem and get much better χ^2 is to increase the maximum temperature, but this results in a quick decrease of the *Differential Emission Measure* with increasing temperature. This result is not satisfactory when a loop model interpretation is attempted, since the *Differential Emission Measure* is expected to monotonically increase with temperature unless very unusual energy input functions are adopted.

This point deserve more attention and will be studied in detail in order to gain information on the energy deposition along the loop.

4.4. The electron density

Examples of the *effective emission measure* (L-functions) versus the electron density are given for Si IX and Mg VIII, just to show the common crossing of the lines. It is possible to see from Fig. 7 that the crossing point of the L-functions is rather well defined, potentially allowing a precise density diagnostics. Mg VIII lines observed in NIS 1 (Fig. 8) are density insensitive in the range 10^9 - 10^{12} cm^{-3} and are potentially diagnostics for coronal hole densities. The Mg VIII L-functions are coincident within the experimental uncertainties for any density greater than 10^8 cm^{-3} (consistently with the Si IX density value measured in

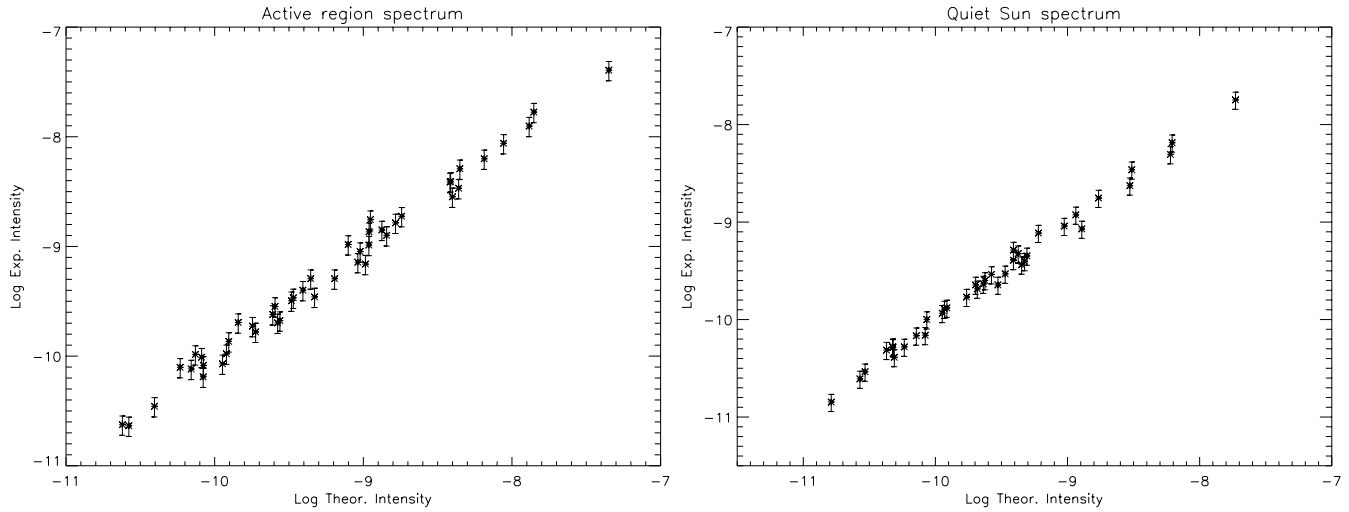

Fig. 6. Comparison between experimental intensities for the lines used in the *Differential Emission Measure* study and their theoretical values computed with *Differential Emission Measure* curves obtained modifying the assumed Feldman 1992 chemical composition. Left: Active region spectrum; Right: Quiet Sun spectrum.

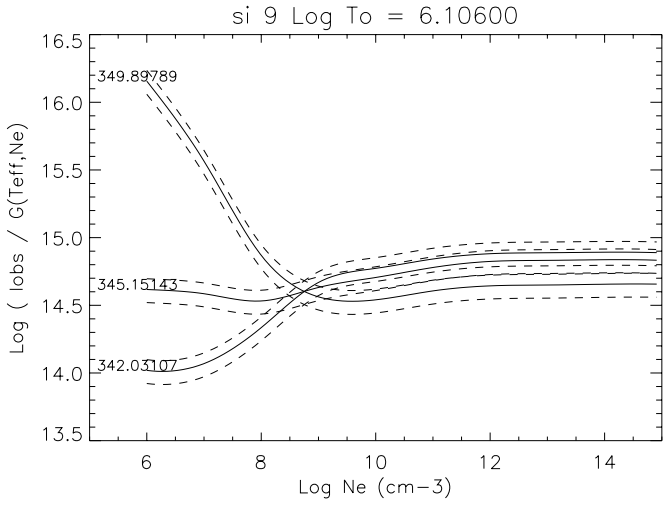

Fig. 7. L-function method for Si IX NIS 1 observed intensities. A density value of Log N_e = $8.7^{+0.4}_{-0.3}$ is indicated.

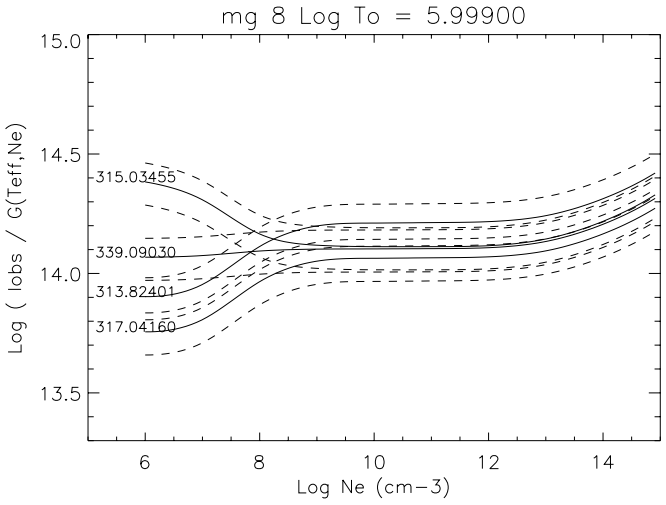

Fig. 8. L-function method for Mg VIII NIS 1 observed intensities. Any log $N_e \geq 8.0$ justifies the observed intensities within the experimental uncertainties.

Fig. 7). It is possible that line 313.8 is blended, as observed by Brooks et al. 1998, though the other component of the blend has not been identified.

We have applied the procedure described in Sect. 2.2 to all the ions whose lines are observed by NIS spectrometer in order to determine the electron density of the emitting plasma as a function of the effective electron temperature T_{eff} associated with each density measurement. We have repeated this study for both the active and quiet regions looking for any difference between their physical conditions.

The CDS NIS spectral range includes density sensitive emission lines from several different ions formed at temperatures ranging from 10^5 K (Ne V) to 2×10^6 K (Fe XV) and therefore potentially allows density diagnostics in a variety of plasma conditions. Nevertheless line blending limits the possibilities of NIS reducing the number of lines really useful for density diagnostics; moreover in quiet Sun conditions the relative weakness of the hot Fe lines limits the precision of the density measurements, while in active Sun the energy levels originating the density sensitive lines in the spectra of some ions come into Boltzmann equilibrium and are of no use for density diagnostics (like Mg VIII and Si IX). Table 2 lists the ions we have used for this study. It is possible to see that these ions are formed in different temperature regimes, from 6×10^5 to 1.5×10^6. This allows us to measure the density versus temperature relation in both quiet and active Sun.

The results for an active and a quiet region are displayed in Fig. 9. The values of the electron density derived for each of the four solar regions are reported in Table 3.

These results need some comments. It is possible to see that the average active region electron densities are about twice the

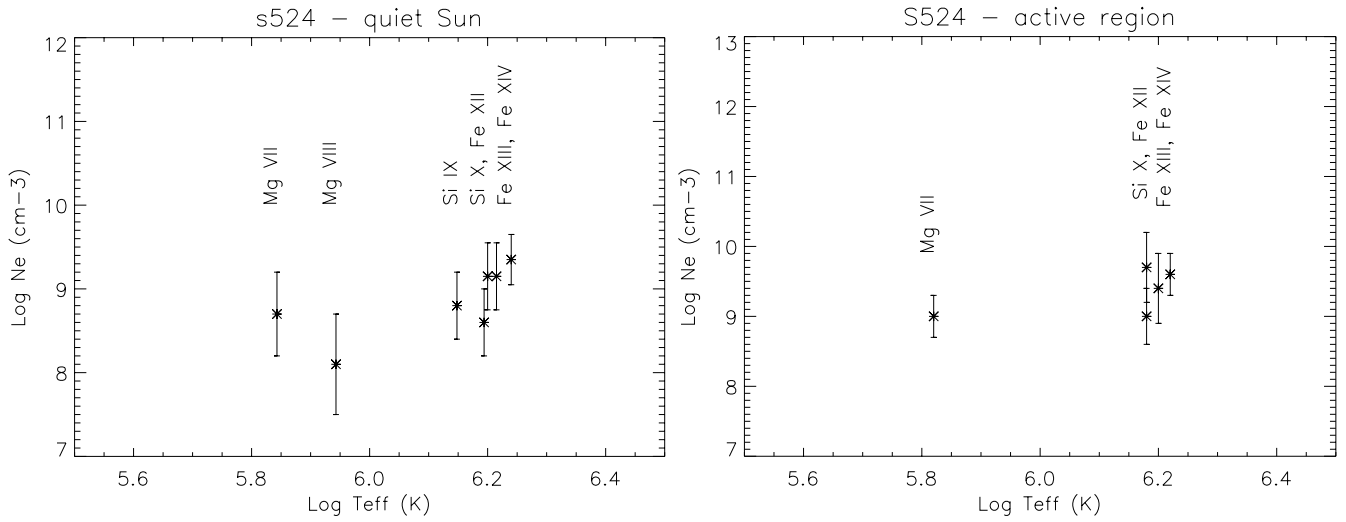

Fig. 9. Left: Electron density measurements for a quiet Sun spectrum as a function of electron temperature. Right: Electron density measurements for an active Sun spectrum as a function of electron temperature. The Mg VII measurement is a bit uncertain in both cases (see text).

Table 2. List of the ions used for density diagnostics. Mg VIII and Si IX NIS lines do not provide any density measurement in active region since they become relatively density insensitive above $10^{9.5}$ cm^{-3}.

Ion	Log T$_{max}$	Quiet Sun	Active Sun
Mg VII	5.8	⋆	⋆
Mg VIII	5.9	⋆	
Si IX	6.0	⋆	
Si X	6.1	⋆	⋆
Fe XII	6.1	⋆	⋆
Fe XIII	6.2	⋆	⋆
Fe XIV	6.3	⋆	⋆

quiet Sun values in the higher temperature region, but all of them show quite large uncertainties. It is possible to see that the Fe XII, XIII and XIV T$_{eff}$ values are very similar so their electron densities are expected to be very similar, as observed, although in quiet Sun spectra there is some difference between Fe XIII and the other ions. Also Si X and Fe XII electron densities are expected to agree since their tef are very similar. Nevertheless it is possible to see that Si X electron density is always smaller than the Fe XII value. This behaviour is observed also in other CDS - NIS spectra and SERTS data (Young et al. 1997, Brosius et al. 1996, Landi & Landini 1997, Young 1997) in a variety of different solar conditions. More recently, Landi et al. 1998 have performed a critical comparison of new Iron Project Fe XII calculations (Binello et al. 1998a and 1998b), CHIANTI data and SERTS-95 observations (Brosius et al. 1998), finding that different calculations yelded very different density values, and yet no agreement was found between densities obtained with any of these calculations and those obtained with other Fe ions. Landi et al. 1998 show that this is due to atomic physics problems and therefore further studies are recommended on Fe XII.

Table 3. Electron density (N_e)measurements for the four analysed solar regions. Mg VIII and Si IX in some cases only allow to determine a lower limit to the electron density. For each ion the upper line reports Log T$_{eff}$ and the lower line the Log N_e measurement.

Ion	Quiet Sun 1	Quiet Sun 2	Active Sun 1	Active Sun 2
Mg VII	5.87	5.84	5.82	5.84
	9.2±0.4	8.7±0.5	9.0±0.3	8.75±0.4
Mg VIII	5.96	5.94	5.93	5.96
	≥8.0	8.1±0.6	≥8.0	≥8.0
Si IX	6.08	6.15	6.15	6.20
	8.7±0.35	8.9±0.4	≥8.5	≥8.5
Si X	6.12	6.19	6.18	6.22
	8.6±0.3	8.8±0.4	9.0±0.4	8.9±0.4
Fe XII	6.12	6.20	6.18	6.21
	9.3±0.4	9.15±0.4	9.7±0.5	9.7±0.4
Fe XIII	6.15	6.22	6.20	6.22
	8.8±0.3	9.15±0.4	9.4±0.5	9.4±0.4
Fe XIV	6.17	6.24	6.22	6.24
	9.35±0.3	9.35±0.3	9.6±0.3	9.5±0.25

The results reported in Table 3 allows also some comment on the density versus temperature relation of the emitting regions. Though there are differences between each of the four regions, all of them show the same behaviour as a function of the effective temperature T$_{eff}$. Table 3 and Fig. 9 indicates that the electron density slightly increases with the effective temperature T$_{eff}$. A similar behaviour has already been observed since a long time and confirmed by SERTS data (Landi & Landini 1997, Young et al. 1998). This behaviour is in contrast with constant

Table 4. Measured ratio between theoretical and experimental intensity for the observed silicon and calcium ions.

Ion	Quiet Sun 1	Quiet Sun 2	Active Sun 1	Active Sun 2
Si III	0.32±0.05	0.36±0.05	0.48±0.06	0.38±0.05
Si VIII	2.8±0.6	3.8±1.0	3.7±1.0	4.4±1.1
Si IX	1.7±0.5	2.3±0.5	2.2±0.5	2.4±0.5
Si X	1.3±0.4	1.5±0.4	1.6±0.4	1.5±0.4
Si XII	1.6±0.4	0.9±0.2	0.9±0.2	1.0±0.2
Ca X	0.27±0.05	0.30±0.05	0.29±0.05	0.35±0.05

pressure assumptions usually done for models of coronal loops. It is important to note however that with the only exception of the second quiet region, the low temperature behaviour is determined only by Mg VII. Mg VII density diagnostics is due to the $2s^2 2p^2\ ^1\mathrm{D}_2$ - $2s2p^3\ ^1\mathrm{D}_2$ transition at 319.03 Å which is density sensitive in the range $10^8 - 10^{10}$ cm^{-3}; the other Mg VII lines observed by the NIS spectrometer ($2s^2 2p^2\ ^3\mathrm{P} - 2s2p^3\ ^3\mathrm{P}$) are only weakly density sensitive. Thomas & Neupert 1994 reported the 319.03 Å line as blended by the Ni XV $3s^2 3p^2\ ^3\mathrm{P}_2$ - $3s3p^3\ ^3\mathrm{D}_3$ line at 319.06; Young et al. 1998 showed that the Ni XV contribution to the observed intensity is not negligible, estimating it to be $\simeq$ 30% of the total. In the present study we do not think that Ni XV provide any significant contribution to Mg VII in quiet Sun, but could be a problem in active Sun. Nevertheless, the presence of Ni XV contribution would lower the value of the electron density measured with the Mg VII 319.03 Å and this gives a further confirmation of the density versus temperature relation described above.

5. Discussion

5.1. Synthetic spectrum

Using the *Differential Emission Measure* distributions determined in Sect. 4.1 the synthetic spectra for both NIS 1 and NIS 2 sections of all the considered regions have been computed. We have adopted $N_e = 1 \times 10^9$ cm^{-3} for quiet Sun and $N_e = 2 \times 10^9$ cm^{-3} for active Sun. No attempt has been made to insert a density versus temperature model in the computation. For this reason some discrepancy between the observed density sensitive lines and their theoretical counterparts is observed for the ions whose measurements of electron density has provided values different from the adopted ones. This provides further evidence for the density variation as a function of temperature in the observed regions.

A general good agreement is observed for both NIS 1 and 2; the Arcetri Spectral Code is able to simulate all the observed lines, with only few exceptions particularly when very weak lines are involved.

The comparison between observed and synthetic spectra provides also evidence that silicon abundance needs some correction, its computed values being systematically larger than the observed ones, and the differences being spatially variable. The measured ratios between theoretical and experimental intensities for the Si ions are reported in Table 4. Since most Si lines are density dependent, they have not been used for *Differential Emission Measure* analysis. In the range of T_{eff} of Si VIII to Si XII the *Differential Emission Measure* is constrained by Fe XI to Fe XVI and the discrepancy seems to suggest that the Si/Fe abundance should be revised, but also some atomic physics problem could be present. Unfortunately silicon V-VII ions lines have not been detected in the present spectrum and therefore it is not possible to check directly whether the Si/Fe discrepancy is extended also to Mg/Si and Ne/Si.

In Table 4 a very different behaviour from the other silicon lines is shown by the Si III $3s^2\ ^1\mathrm{S}_0$ - $3s4p\ ^1\mathrm{P}_1$ transition observed at 566.6 Å; its theoretical intensity is too low to account for all the observed counterpart. One possibility is that this line is blended with some other line, though the CHIANTI database and the Arcetri spectral code have no candidates for this wavelength. This line should provide roughly 2/3 of the total observed intensity. Si III $\mathrm{T}_{eff}$is instead very close to the He I and II values and therefore its intensity is compared to that of these ions. The formation of the helium spectrum is not well understood (Andretta & Jones 1997 and references therein) and a simple optically thin model like the one adopted in the present calculation may not be adequate. This may cause the observed discrepancy.

5.2. Chemical composition

Magnesium and neon relative abundances have been studied in the past because it is possible to simultaneously observe EUV lines emitted by some of their ions formed at very similar temperatures. This allows direct comparison of their abundance, and it is of interest since magnesium is a low-FIP element while neon is a high-FIP element, and the FIP effect (e.g Haisch et al. 1996) can therefore be investigated. In the present work the disagreement between the adopted coronal Feldman 1992 abundances and observations shows that the FIP effect in the observed regions is less active than assumed by using Feldman 1992 abundances. Moreover, the importance of the FIP effect changes in the different regions, as witnessed by the different corrections required by the *Differential Emission Measure* in Sect. 4.1.

Variations of neon and magnesium abundances have been reported by Young & Mason 1997, finding that the Ne/Mg relative abundance changed by a factor 9 in two solar brightenings observed with CDS. These variations are much higher than those found in the present work. High Mg/Ne ratios are associated with spike-like structures extending outwards from active regions, while low Mg/Ne abundance values are associated to emerging flux regions (Sheeley 1996). The measurements found in the present work seem to follow this trend, as the observed region does not present any spike-like structure, and is associated to emerging magnetic flux. The large variability of the Ne/Mg abundance ratio is also discussed in Widing & Feldman 1993 and 1995, where several different active regions were analyzed. The Ne/Mg abundance ratio has been found to change by a factor 6 relatively to its photospheric value. On the contrary, the Ne/O abundance ratio changes by a factor $\leq$ 1.5 and this variation has large experimental uncertainties. Thus, as found

in the present work, neon and oxygen (both high-FIP elements) seem to maintain their relative photospheric abundance.

Falconer 1997 report that in SERTS spectra aluminum abundance was enhanced relative to the low-FIP elements, confirming the proposed two-step enrichment mechanism for the FIP effect proposed by Feldman 1992, so that very low-FIP elements such as aluminum are enhanced first, and in the second step all the rest of low-FIP elements are increased by the same amount. Widing & Feldman 1993 also discuss changes in sodium abundances, finding that the two-step FIP model could be confirmed by observations, although experimental uncertanties prevented the authors from giving more precise measurements.

In the present work no signature is found of this process, since Al X and Al XI lines agree well with other elements. Moreover, CDS-NIS spectral resoluton do not allow to resolve the very low-FIP Na VII lines at around 350 Å, so that we cannot say more on the two-step FIP model from the present spectrum.

Also the calcium abundance shows some problem, since the two sodium-like Ca X lines observed at 557.7 Å and at 574.0 Å always show a too high theoretical intensity, suggesting a large discrepancy between the adopted calcium abundance and the real value. There is no evidence of abundance variations with position. Interestingly, the blending C III 574.3 Å $2s2p\ ^1\mathrm{P}_1$-$2s3d\ ^1\mathrm{D}_2$ line seems to provide a negligible contribution to the total intensity of the calcium line. Table 4 suggests that the adopted abundance for calcium should be enhanced approximately by a factor three. This result points in the same direction as Widing & Feldman 1993.

Raymond (1998) reports that also ionization equilibrium could play an important role into this disagreement, and that improved ionization and recombination rates are needed to help solving the calcium disagreement. This is further confirmed by the analysis of SERTS-95 Ca XIV, Ca XV and Ca XVII lines in the 180-210 Å spectral range (Brosius et al. 1998a, 1998b), showing large disagreements with lines of ions formed at similar temperatures, which cannot be solved by a simple element abundance correction. Further calculations on calcium ionization equilibrium are recommended.

5.3. Electron density

The electron density- electron temperature relation is of great importance for the understanding of the physics of the structures ruling the solar corona. In the recent past, the advent of high quality instruments, such as SERTS and SOHO-CDS, has permitted to study density diagnostics as a function of the temperature of formation of the emitting ion. In several cases a similar relation to the one found in the present work is found.

Young et al. 1998 report a very detailed study of the SERTS 1989 observation (Thomas & Neupert 1994) with the aim of comparing the CHIANTI database with SERTS observation: as a by-product of their analysis electron density diagnostics is performed for temperatures greater than $10^{5.4}$ K, including also transition region lines. Young et al. 1998 measurements reveal that the electron density shows the same behaviour as found in the present work. It is important to note however that the spectrum the authors analyzed is obtained averaging the emission of the whole SERTS slit, which covered quiet Sun, active region and a small subflare. Thus the emitting region is dishomogeneous and the derived density-temperature relation has little meaning. On the contrary Landi & Landini 1997 derive a very similar result using the spectrum obtained averaging the SERTS-89 emission recorded by the slit pixels corresponding to the active region only. It is also interesting to note that the low values for the transition region electron densities obtained by Landi & Landini 1997 and Young et al. 1998 are in disagreement with the measurements obtained with O IV and O V in solar and stellar spectra (Cook et al. 1995, Keenan et al. 1995), whose values are greater than 10^{10} cm^{-3}. These ions are all formed at the same temperature, and they are expected to provide the same values for the electron density.

Brickhouse et al. 1995 analyze SERTS-89 and EUVE observations of Fe lines from the Sun and Capella. From their work electron densities are measured at coronal temperatures using Fe IX-XV ions, finding that the average densities provided by Fe ions is approximately constant. It should be noted however that they report density measurements from *all* the available ratios of each iron ion, without a preliminary selection of lines not affected by blending or atomic physics problems: for this reason the density values provided by each ion extend over two orders of magnitude and create some confusion. Also Brosius et al. 1996 determine electron densities from SERTS observations of solar active and quiet regions using the 1991 and 1993 flights. Again, the slit covered different regions; no significant trend was found for the electron density as a function of the electron temperature.

In all these cases, the measured density versus temperature relation is is disagreement with constant-pressure models, so that much more complex models for the emitting plasma are required. A similar conclusion has been found by Feldman & Laming 1993, reporting that the costant pressure assumption was not reproduced by Skylab observation of active regions for temperatures between 5×10^4 and 2×10^5 K. The authors report that a constant density assumption is better justified by the observations. Although the temperature range is different from the one covered by the spectra analyzed in the present study, confirms that the solar atmosphere has a very complex behaviour and a simple constant pressure model cannot account for it.

6. Conclusions

We have analyzed two pairs of active and quiet Sun regions, determining their *Differential Emission Measure* distribution, the electron density of each of these regions as a function of electron temperature. Some corrections to the Feldman abundances of neon, oxygen are evaluated, and suggestions also for silicon and calcium are given. Use has been made of the Arcetri diagnostic technique for the analysis; this technique allows also to constrain the *Differential Emission Measure* to have a maximum temperature T_{max}. A peak temperature of 1.6×10^6 K and

electron density of 10^9 cm^{-3} are obtained for quiet Sun and 2.0×10^6 K and 2×10^9 cm^{-3} for the active regions.

For this kind of study a large quantity of high quality atomic data is required. In recent times some extensive databases have been created for matching the increasing need of theoretical transition probabilities, such as ADAS (Summers et al. 1996) and CHIANTI (Dere et al. 1997). In the present study we made use of the Arcetri Spectral Code (Landi & Landini 1998) which is an updating of the old version (Monsignori Fossi & Landini 1996) using the CHIANTI database and additional data for ions not yet included in the CHIANTI database.

References

Andretta, V., Jones, H.P., 1997, ApJ, 489, 375

Arnaud, M. & Raymond, J.C., 1992, ApJ, 398, 394.

Arnaud, M. & Rothenflug, R., 1985, A&ASS, 60, 425.

Binello, A.M., Mason, H.E., Storey, P.J., 1997, Adv.Sp.Res., 20, 2263

Binello, A.M., Mason, H.E., Storey, P.J., 1998, A&ASS, 127, 545

Brickhouse, N.S., Raymond, J.C., Smith, B.W., 1995, ApJSS, 97, 551

Brooks,D.H., Fischbacher, G., Fludra, A., Harrison, R., Innes, D., Lang, J., Landi, E., Landini, M., Lanzafame, A., Loch, S., McWhirter, R.W.P., Summers, H.P., Thompson, W., 1998, A&A, submitted.

Bromage, B.J.I., Breeveld, A.A., Kent, B.J., Pike, C.D. & Harrison, R.A.: 1996, *UCLan Report CFA/96/09*.

Brosius, J.W., Davila, J.M., Thomas, R.J., Monsignori Fossi, B.C., 1996, ApJSS, 106, 143.

Brosius, J.W., Davila, J.M., Thomas, R.J., 1998a, ApJ, *in press*

Brosius, J.W., Davila, J.M., Thomas, R.J., White, S.M., 1998b, AGU meeting, SM52A-08, Boston (Ma), 26-29 May 1998

Cook, J.W., Keenan, F.P., Dufton, P.L. et al., 1995, ApJ, 444, 936

Dere, K.P., Landi, E., Mason, H.E., Monsignori Fossi, B.C. & Young, P.R.: 1997, *Astr. Astrophys. Suppl. Ser.*, 125, 149.

Falconer, D.A., Davila, J.M., Thomas, R.J., 1997, ApJ, 482, 1050

Feldman, U., 1992, Phys. Scripta, 46, 202

Feldman, U., Laming, J.M., 1993, ApJ, 404, 799

Haisch, B., Saba, J.L.R., Meyer, J-P., 1996, in *Preceedings of the 9^th Cambridge workshop on Cool Stars, Stellar systems and the Sun*, eds. R. Pallavicini & A.K. Dupree, ASP Conf Series 109, p. 511

Harrison, R.A. & Thompson, A.M. (eds.), 1992, *Intensity integral inversion techniques: a study in preparation for the SOHO mission*, RAL-91-092, Rutherford Appleton Laboratory.

Harrison, R.A., Sawyer, E.C., Carter, M.K. et al., 1995, *Solar Physics*, 162, 233.

Keenan, F.P., Brekke, P., Byrne, P.B., Greer, C.J., 1995, MNRAS, 276, 915

Landi, E. & Landini, M., Paper I, 1997, *Simultanous temperature and density diagnostics of optically thin plasmas*, A&A, 327, 1230

Landi, E. & Landini, M., 1998, *The Arcetri Spectral Code*, A&ASS, *in press*

Landi, E., Landini, M., Pike, C.D., Mason, H.E., 1997, Sol. Phys., 175, 553

Landi, E., Binello, A.M., Brosius, J.W., 1998, A&A, *in preparation*

Landini, M. & Monsignori Fossi, B.C., 1975, A&A, 42, 213.

Landini, M. & Monsignori Fossi, B.C., 1991, A&ASS, 91, 183.

Monsignori Fossi, B.C., Landini, M., 1996, in *Astrophysics in the Extreme Ultraviolet*, Kluwer Ac. Pub, eds. S. Bowyer & R.F. Malina, p. 543.

Raymond, J.C., 1998, *Private Communications*

Sheeley, N.R., 1996, ApJ, 469, 423

Summers,H.P., Brooks, D.H., Hammond, T.J., Lanzafame, A.C. & Lang, J., 1996, RAL Technical Report RAL-TR-96-017, March 1996

Thomas, R.J., Neupert, W.M., 1994, ApJSS, 91, 461

Widing, K.G., Feldman, U., 1993, ApJ, 416, 392

Widing, K.G., Feldman, U., 1995, ApJ, 442, 446

Young, P.R., Landi, E., Thomas, R.J., 1998, A&A, 329, 291

Young, P.R., Mason, H.E., 1997, Sol. Phys., 175, 523

Young, P.R., 1997 *Private communications*